Temperature dependent carrier lifetime studies of Mo in crystalline silicon

Bijaya B. Paudyal,[1,a)] Keith R. McIntosh,[1] Daniel H. Macdonald,[2] and Gianluca Coletti[3]
[1]*Centre for Sustainable Energy Systems, Australian National University, Canberra, Australian Capital Territory 0200, Australia*
[2]*Department of Engineering, College of Engineering and Computer Science, Australian National University, Canberra, Australian Capital Territory 0200, Australia*
[3]*ECN Solar Energy, Energy research Centre of Netherlands, NL-1755 LE Petten, The Netherlands*

The capture cross sections of both electrons σ_n and holes σ_p were determined for interstitial molybdenum in crystalline silicon over the temperature range of -110 to $150\ °C$. Carrier lifetime measurements were performed on molybdenum-contaminated silicon using a temperature controlled photoconductance instrument. Injection dependent lifetime spectroscopy was applied at each temperature to calculate σ_p and σ_n. This analysis involved a novel approach that independently determined the capture cross sections at each temperature assuming a known defect density and thermal velocity. Since the energy state is in the lower half of the bandgap, the determination of σ_p is unaffected by the defect energy at all temperatures, and σ_p is found to decrease with temperature in a fashion consistent with excitonic Auger capture. At temperatures below $0\ °C$, the determination of σ_n is also unaffected by the defect energy due to the suppression of thermal emission, and σ_n decreases with temperature as well. It is shown that a projection of σ_n to higher temperature suggests the defect has an energy of 0.375 eV above the valance band edge of silicon. © *2010 American Institute of Physics*. [doi:10.1063/1.3309833]

I. INTRODUCTION

Molybdenum (Mo) is a transition metal and a potential source of contamination in silicon devices.[1] Mo remains in interstitial form within the lattice structure of silicon and creates an electrically active defect. Istratov *et al.*[2] measured significant amounts of Mo in commercially available multicrystalline silicon for solar cells, while Davis *et al.*[3] showed Mo to have a very strong impact on solar cell efficiency in Cz silicon, reducing it by up to one third.

In 1995, Graff[1] summarized published information about the electrical properties of Mo in silicon, mostly based on deep level transient spectroscopy (DLTS). Interstitial Mo was found to introduce a single defect energy level (E_t) that is donorlike and exists at 0.28 ± 0.01 eV above the valance band edge of silicon (E_V) with hole and electron capture cross sections $\sigma_p = 6.0 \times 10^{-16}\ cm^2$ and $\sigma_n = 1.60 \times 10^{-14}\ cm^2$, respectively. In addition to those studies, Rohatgi *et al.*[4] applied DLTS coupled with dark and illuminated I-V measurements and concluded the defect energy to be $E_t = E_V + 0.30$ eV. Hamaguchi *et al.*[5] applied DLTS and optical-DLTS to investigate the Mo-related defects in silicon and reported $E_t = E_V + 0.31$ eV. Similarly Pettersson *et al.*[6] applied junction space charge techniques (JSCTs) and found $E_t = E_V + 0.298$ eV. More recently, Rein *et al.*[7,8] applied a combination of temperature and injection dependent lifetime spectroscopy to determine $E_t = E_V + 0.317 \pm 0.05$ eV and the ratio of the capture cross sections $\sigma_n / \sigma_p = 13 \pm 3$. Furthermore, they concluded that both σ_p and σ_n have a dependence on temperature of $T^{-1.5}$, where it was assumed that the temperature dependence of σ_n / σ_p was constant. In this work, we explicitly measure the temperature dependence of both σ_p and σ_n, from which we also determine the temperature dependent trend of σ_n / σ_p. Furthermore, the measured temperature dependence of σ_n is used to assess E_t of Mo in silicon. Table I summarizes these published results on the interstitial Mo defect in Si.

This paper presents a novel and relatively simple technique to determine $\sigma_p(T)$ and $\sigma_n(T)$ over a wide range of temperature. It employs injection-dependent lifetime spectroscopy with a T-controlled photoconductance (PC) measurement instrument. Section II explains the carrier lifetime theory and its simplification in order to determine the temperature-dependent expression for $\sigma_p(T)$ and $\sigma_n(T)$, and the application of $\sigma_n(T)$ to determine E_t. This is followed by Sec. III that presents the preparation of Mo-contaminated samples for this work, the instrument and the details of the measurement procedure. In Sec. IV, we present $\sigma_p(T)$ and $\sigma_n(T)$, and analyze their trends to give insight into the effective capture mechanism and to assess E_t.

II. THEORY

The simplified version of Shockley Read Hall (SRH) lifetime[9,10] for a single defect can be written as[11]

$$\tau_{SRH} = \frac{\tau_{n0}(p_1 + p_0 + \Delta n) + \tau_{p0}(n_1 + n_0 + \Delta n)}{(n_0 + p_0 + \Delta n)}, \quad (1)$$

where τ_{n0} and τ_{p0} are the fundamental capture time constants for electrons and holes, $n_1 = N_c \exp[-(E_c - E_t)/k_B T]$ and $p_1 = N_v \exp[-(E_t - E_v)/k_B T]$, N_c and N_v are the effective densities of states at the conduction and the valance band edge, k_B is the Boltzmann's constant, n_0 and p_0 are the electron and hole densities at thermal equilibrium, and Δn is the excess

a)Electronic mail: bijaya.paudyal@anu.edu.au.

TABLE I. Summary of published results for interstitial molybdenum in crystalline silicon. The table lists the capture cross section of electrons σ_n and holes σ_p, and the defect energy E_t above the valence band edge E_v.

σ_p (cm^2)	σ_n (cm^2)	σ_n/σ_p at 27 °C	E_t (eV)	Ref. and technique
6.0×10^{-16} at 27 °C	1.6×10^{-14} at 27 °C	26.67	$E_v + 0.28$	DLTS,[a] average
NA	NA	NA	$E_v + 0.31$	DLTS[b]
NA	NA	NA	$E_v + 0.30$	DLTS[c]
NA	7.8×10^{-15} at 27 °C	13.0	$E_v + 0.317$	TIDLS[d]
NA	NA	NA	$E_v + 0.298$	JSCT[e]
$6.05 \times 10^{-14} \times T^{-1.07}$	$4.21 \times 10^{-8} \times T^{-2.95}$	11 ± 2	$E_v + 0.375 \pm 0.03$	This work, TIDLS

[a]Reference 1.
[b]Reference 5.
[c]Reference 4.
[d]References 7 and 8.
[e]Reference 6.

carrier density. Equation (1) assumes that trapping effects are negligible (i.e., $\Delta n = \Delta p$).[11]

For a p-type wafer, n_0 can be neglected in comparison with p_0 and when Δn is sufficiently less than p_0, τ_{SRH} can be rewritten as

$$\tau_{SRH} = \frac{\tau_{n0}(p_1 + p_0) + \tau_{p0}(n_1 + n_0)}{p_0} + \frac{\tau_{p0}}{p_0}\Delta n. \quad (2)$$

At a sufficiently low temperature, emission from the defect energy level is negligible and $n_1(T) + n_0(T) \ll \Delta n$ and $p_1(T) \ll p_0(T)$. In such a case, Eq. (2) can be simplified further to become

$$\tau_{SRH} = \tau_{n0} + \frac{\tau_{p0}}{p_0} \times \Delta n. \quad (3)$$

Figure 1 presents a plot that shows the temperature below which Eq. (3) is valid. It plots T when $n_1 + n_0 = 0.01 \times \Delta n = 0.0001 \times p_0$ and when $p_1 = 0.01 \times p_0$ as a function of E_t and N_A. It assumes $n_1 + n_0$ negligible in comparison to Δn when earlier's value is less than 1% of the latter and a similar assumption applies to p_1 and p_0. At temperatures below the lines in Fig. 1 (for a given N_A), it is safe to employ Eq. (3). The figure shows that the temperature below which both assumptions are valid decreases as (i) N_A decreases and (ii) as the defect energy level moves further from midgap. The latter occurs because thermal emission from a defect level to a
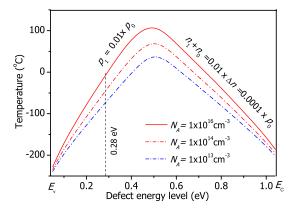

FIG. 1. (Color online) Temperature below which $n_1 + n_0 = 0.01 \times \Delta n = 0.0001 \times p_0$ and $p_1 = 0.01 \times p_0$ as a function of E_t for p-type silicon of three doping densities (N_A).

band edge is high when the defect energy is near that band edge.

At temperatures where Eq. (3) is valid, the slope of a plot of τ_{SRH} against Δn gives τ_{p0}/p_0 and the intercept gives τ_{n0}. Hence σ_n and σ_p can be calculated using the measured slope and the intercept of a linear plot of τ_{SRH} against Δn for different temperatures, as

$$\sigma_p = \frac{1}{\tau_{p0}v_{thp}N_t} = \frac{1}{\text{Slope} \times p_0 v_{thp}N_t}, \quad (4)$$

$$\sigma_n = \frac{1}{\tau_{n0}v_{thn}N_t} = \frac{1}{\text{Intercept} \times v_{thn}N_t}, \quad (5)$$

where v_{thp} and v_{thn} are the thermal velocities of holes and electrons and N_t is the defect concentration. In some cases the effective capture mechanism can be inferred from the temperature dependence of $\sigma_n(T)$ and $\sigma_p(T)$.[12–14]

At higher temperatures, when carrier emission from the defect energy level is significant and $n_1(T) + n_0(T)$ is not negligible compared with Δn or $p_1(T)$ is not negligible in comparison to $p_0(T)$, the more generalized expression of Eq. (2) must be employed. In such a case, the slope of a plot of τ_{SRH} against Δn is still $\tau_{p0}(T)$ and Eq. (4) remains a valid way to determine $\sigma_p(T)$. However, the intercept of the plot becomes a function of $p_1(T)$ and/or $n_1(T)$, which are dependent upon E_t. Therefore, a value of E_t is required to calculate $\sigma_n(T)$ at higher temperatures. By extrapolating the observed trend of $\sigma_n(T)$ measured at lower temperatures, and assuming the dominant capture mechanism remains unchanged as the temperature increases, it is therefore possible to determine the energy level itself.

III. EXPERIMENT

A silicon ingot was grown with the pedestal growth technique and boron-doped with a resistivity of 1.8 Ω cm. The ingot was intentionally contaminated by adding 2800 ppma of molybdenum (Mo) in the silicon melt.[15] A Mo concentration of 2×10^{13} cm^{-3} was determined by neutron activation analysis (NAA) on the section of the ingot studied here, as described in detail elsewhere.[15] If all of the Mo atoms are interstitial and active, this gives an upper limit to N_t of 2×10^{13} cm^{-3}. The experiment was performed on a silicon
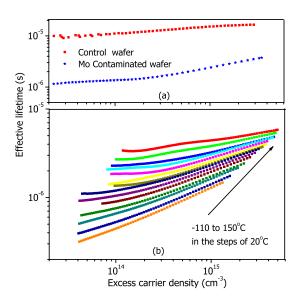
FIG. 2. (Color online) (a) Measured lifetime of the Mo-contaminated and control wafers at room temperature. (b) Measured lifetime of Mo-contaminated wafer for temperatures of −110 to 150 °C.

sample sliced from the ingot. The wafer was subject to a phosphorus diffusion step, to remove unintended fast-diffusing impurities such as Fe, which may otherwise affect the lifetime. The diffused layers were then removed by chemical polishing, followed by cleaning and a plasma enhanced-chemical vapor deposited, SiN_x layer optimized for surface passivation as described by Coletti *et al.*[16] The average width of the sample was 285 μm.

Lifetime measurements were performed on a temperature controlled inductive coil PC based instrument, described in detail elsewhere.[17] Figure 2(a) depicts the injection dependent lifetime data for the Mo-contaminated wafer and a control wafer at room temperature, and Fig. 2(b) presents injection dependent lifetime data for the Mo-contaminated wafer for −110 to 150 °C. The effective lifetime (τ_{eff}) in the Mo-contaminated wafer was found to be an order of magnitude smaller than the control wafer, which indicates that the Mo impurities have a dominant effect on overall recombination. We therefore assume the measured quantity τ_{eff} is equal to the τ_{SRH} that is associated with interstitial Mo in these samples.
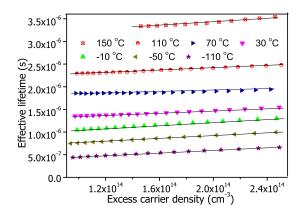
The quasisteady-state PC technique[18] was employed to

FIG. 3. (Color online) Lifetime plot and linear fit of Mo-doped (1.8 Ω cm) wafer for the selected injection range ($1 \times 10^{14} - 2. \times 10^{14}$ cm^{-3}).
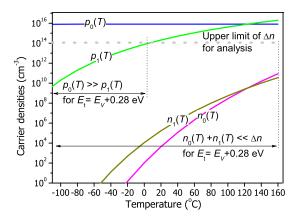

FIG. 4. (Color online) Carrier densities (n_1, p_1, n_0, and p_0) for a defect energy level ($E_V + 0.28$ eV).

determine the carrier lifetime at different temperatures. The carrier mobility model developed by Reggiani *et al.*[19] was applied for the subsequent analysis of the measured lifetime data. This mobility model accounts for the effect of temperature and dopant concentration but does not account for the effect of Δn. The Reggiani model for carrier mobility was therefore modified by replacing the donor density N_D with $N_D + \Delta n$ and the acceptor density N_A with $N_A + \Delta n$. This approximation was found to give a good agreement with the mobility model of Klaassen *et al.*[20,21] at room temperature. Reggiani's carrier mobility model was preferred in this case because of it validity over a larger temperature range (−73 to 327 °C). The temperature across the wafers was found to vary by ±2% during measurement and the uncertainty in the measured lifetime was ±6%,[17] which depends mostly upon the calibration of the illumination intensity and the inductive coil. The effective lifetime τ_{eff} was measured as a function of Δn over a temperature range of −110 to 150 °C at intervals of 10 °C. Figure 3 depicts the measured τ_{eff} as a function of Δn from −110 to 150 °C in steps of 40 °C.

When $\Delta n < 2.5 \times 10^{14}$ cm^{-3}, the above mentioned conditions of Eqs. (2) and (3) are satisfied. The carrier densities (n_1, p_1, n_0, and p_0) and Δn for the analysis are depicted in Fig. 4 for the defect energy level of $E_V + 0.28$ eV in silicon. This graph shows $n_1 + n_0 \ll 1 \times 10^{14}$ cm^{-3} for temperatures less than 160 °C and $p_1 \ll p_0$ for temperatures less than 0 °C. Table II depicts the temperature ranges for which the assumption $(n_1 + n_0) \ll \Delta n$ and $p_1 \ll p_0$ is valid for different reported values of E_t, where we require $(n_1 + n_0)$ and p_1 to be no more than 1% of Δn and p_0, respectively. In this work, we choose the most conservative upper limit of temperature for the subsequent analysis, as represented by the vertical line in Fig. 1. $n_0(T)$ was determined by using the doping density

TABLE II. Upper limit of T_{low}(°C) for which the assumptions $(n_1 + n_0) < 0.01 \times \Delta n$ and $p_1 < 0.01 \times p_0$ is valid for analysis.

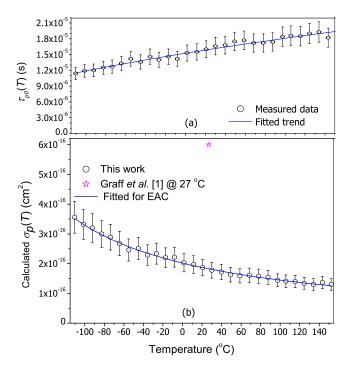| E_t (eV)	$(n_1 + n_0) \ll \Delta n$ (°C)	$p_1 \ll p_0$ (°C)	Ref.
$E_V + 0.28$	$T \leq 160$	$T \leq 0$	1
$E_V + 0.30$	$T \leq 158$	$T \leq 10$	4
$E_V + 0.317$	$T \leq 155$	$T \leq 18$	7 and 8

FIG. 5. (Color online) Measured τ_{p0} (a) and calculated $\sigma_p(T)$ for Mo impurities in silicon (b) with an EAC mechanism fit, depicting other previously published values at RT.

IV. RESULTS AND DISCUSSION

Figure 5(a) plots the measured $\tau_{p0}(T)$ over the temperature range of -110 to $150\,^\circ$C and Fig. 5(b) plots $\sigma_p(T)$ calculated with Eq. (4) assuming that N_t equals the Mo concentration. The figure shows that σ_p decreases with temperature over the entire temperature range. This eliminates the possibility that hole capture occurs via multiphonon emission in which σ_p increases with temperature.[12] We also rule out cascade capture as a possible capture mechanism because it is only relevant to shallow Coulomb attractive defect centers.[14] This leaves excitonic Auger capture (EAC) (Ref. 13) as the most likely mechanism for the capture of holes by the Mo defect.

The temperature dependence of σ under EAC is governed by the equation, $\sigma = \sigma_0 T^\alpha$, where σ_0 and α are independent of temperature. The line in Fig. 5 is a fit of this equation to the experimental data, where $\sigma_0 = 6.05 \pm 0.8 \times 10^{-14}$ cm^{-2} and $\alpha = -1.07 \pm 0.05$. The uncertainty in these values represents a 95% confidence interval from an error-weighted least-square fit to the experimental data.

The above calculation assumes 100% of the Mo atoms, determined by NAA measurements, are electrically active, however this may not be valid if, for example, precipitation occurs[1] or in cas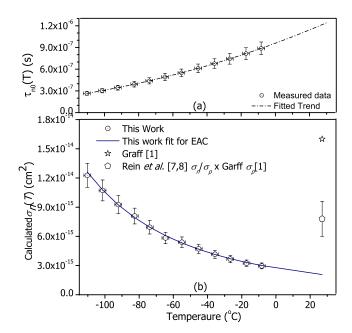e of uncertainties in NAA measurement. In the case where only a fraction f_{act} of Mo atoms are electrically active, the temperature dependence of the hole capture cross section is therefore

$$\sigma_p(T) = \frac{1}{f_{\text{act}}}(6.05 \pm 0.8 \times 10^{-14})T^{-(1.07 \pm 0.05)}. \qquad (6)$$

Thus, σ_0 is inversely proportional to f_{act}, while α is independent of f_{act}. If the fraction of electrically active impurities were $f_{\text{act}} = 0.3$, σ_p becomes consistent with the DLTS value reported by Graff at room temperature.[1] We note that a fractional activation of Mo atoms does not alter the conclusion that EAC is the most likely capture mechanism of holes.

The electron capture cross section $\sigma_n(T)$ was first determined for the temperature range of -110 to $0\,^\circ$C by implementing Eq. (5), which does not require E_t. σ_n is also found to decrease monotonically and like σ_p, it can be best described by an EAC mechanism. The EAC fit of the measured σ_n gives

$$\sigma_n(T) = \frac{1}{f_{\text{act}}}(4.21 \pm 0.4 \times 10^{-8})T^{-(2.95 \pm 0.02)}. \qquad (7)$$

Figure 6(a) shows the measured $\tau_{n0}(T)$ over the temperature range of -110 to $0\,^\circ$C and Fig. 6(b) shows the calculated $\sigma_n(T)$ when $f_{\text{act}} = 1$. When $f_{\text{act}} = 0.3$, σ_n extrapolated to room temperature is consistent with Rein's value of σ_n/σ_p multiplied by Graff's value of σ_p, and when $f_{\text{act}} = 0.15$, σ_n is consistent with Graff's value of σ_n.

Temperature-dependent values of σ_n for the higher temperature range ($0-150\,^\circ$C) were then calculated using various reported values of E_t for Mo[1,4,7,8] as required in Eq. (2). Figure 7(a) depicts the measured intercepts and Fig. 7(b) shows the corresponding $\sigma_n(T)$ calculated for different E_t. This reveals that an energy level of $E_t = E_V + 0.375 \pm 0.03$ eV is required to fit the measured intercept for the extended trend of $\sigma_n(T)$ when we assume the EAC
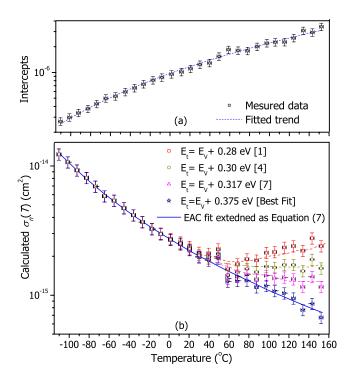

FIG. 6. (Color online) Measured τ_{n0} (a) and calculated $\sigma_n(T)$ for Mo impurities in silicon (b) with an EAC mechanism fit, depicting other previously published values at RT.

FIG. 7. (Color online) Measured intercepts of plot (τ_{eff} vs Δn) (a) and calculated $\sigma_n(T)$ for Mo for previously reported values of E_t. Depicts the best fit with $E_t=E_v+0.375$ eV for EAC mechanism.

mechanism described by Eq. (7) remains dominant. It is possible, however, that the EAC mechanism does not remain dominant and another recombination mechanism that causes $\sigma_n(T)$ to increase with temperatures becomes significant at temperatures above 0 °C. We therefore do not discount the possibility that E_t is smaller than $E_v+0.375$ eV and closer to values determined by other authors[1,4,7,8]

Figure 8 plots the ratio of the capture cross sections (σ_n/σ_p) over the temperature range, -110 to 150 °C. The symbols in Fig. 8 plot the data assuming $E_t=E_v+0.375$ eV, and the error bars combine the uncertainty in the measurement with the uncertainty in E_t. The figure shows that σ_n/σ_p decreases with temperature, even though both carriers are best described by the same capture mechanism (EAC). The data agrees well with the value reported by Rein *et al.*[7,8] at
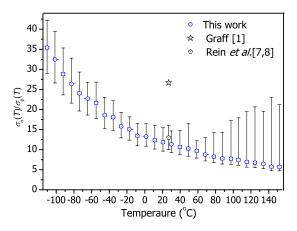

FIG. 8. (Color online) Capture cross section ratio of Mo defect in silicon at different temperatures.

room temperature. The uncertainty due to any partial activation of Mo atoms in silicon [represented by f_{act} in Eqs. (6) and (7)] cancels in the calculation of σ_n/σ_p. However the uncertainty in σ_n/σ_p increases at higher temperature (>0 °C) due to the uncertainty in σ_n associated with the uncertainty in E_t.

V. CONCLUSIONS

Temperature-dependent expressions for σ_n and σ_p of interstitial molybdenum in silicon were independently determined over the temperature range, -110 to 150 °C, using a temperature controlled PC instrument. The T-dependent trends of σ_p and σ_n are best matched by an EAC mechanism, giving minimum values of the coefficients of $\sigma_0=6.1\pm0.8 \times 10^{-14}$ and $4.2\pm0.4\times10^{-8}$ cm^2 and giving T-exponents of $\alpha=1.07\pm0.05$ and 2.95 ± 0.2. Assuming the EAC mechanism also dominates electron capture at higher temperatures, the energy level of interstitial Mo in silicon is determined to be 0.375 ± 0.03 eV above the valance band of silicon.

[1]K. Graff, *Metal Impurities in Silicon-Device Fabrication* (Springer-Verlag, Berlin, 1995).
[2]A. A. Istratov, T. Buonassisi, R. J. McDonald, A. R. Smith, R. Schindler, J. A. Rand, J. P. Kalejs, and E. R. Weber, J. Appl. Phys. **94**, 6552 (2003).
[3]J. R. Davis, Jr., A. Rohatgi, R. H. Hopkins, P. D. Blais, P. Rai-Choudhury, J. R. McCormick, and H. C. Mollenkopf, IEEE Trans. Electron Devices **27**, 677 (1980).
[4]A. Rohatgi, R. H. Hopkins, J. R. Davis, R. B. Campbell, and H. C. Mollenkopf, Solid-State Electron. **23**, 1185 (1980).
[5]T. Hamaguchi and Y. Hayamizu, Jpn. J. Appl. Phys., Part 2 **30**, L1837 (1991).
[6]H. Pettersson, H. G. Grimmeiss, L. Tilly, K. Schmalz, K. Tittelbach, and H. Kerkow, Semicond. Sci. Technol. **6**, 237 (1991).
[7]S. Rein, *Lifetime Spectroscopy: A Method of Defect Characterization in Silicon for Photovoltaic Applications* (Springer, New York, 2005).
[8]S. Rein, S. Diez, and S. W. Glunz, Proceedings of the 19th EC PVSEC, Paris, France, 2004 (unpublished), pp. 219–222.
[9]W. Shockley and W. T. Read, Phys. Rev. **87**, 835 (1952).
[10]R. N. Hall, Phys. Rev. **87**, 387 (1952).
[11]A. G. Aberle, The University of New South Wales (1999).
[12]C. H. Henry and D. V. Lang, Phys. Rev. B **15**, 989 (1977).
[13]A. Hangleiter, Phys. Rev. B **37**, 2594 (1988).
[14]M. Lax, Phys. Rev. **119**, 1502 (1960).
[15]G. Coletti, L. J. Geerligs, P. Manshanden, C. Swanson, S. Riepe, W. Warta, J. Arumughan, and R. Kopecek, Solid State Phenomena **131**, 15 (2008).
[16]G. Coletti, R. Kvande, V. D. Mihailetchi, L. J. Geerligs, L. Arnberg, and E. J. Øvrelid, J. Appl. Phys. **104**, 104913 (2008).
[17]B. B. Paudyal, K. R. McIntosh, D. H. Macdonald, B. S. Richards, and R. A. Sinton, Prog. Photovoltaics **16**, 609 (2008).
[18]R. A. Sinton and A. Cuevas, Appl. Phys. Lett. **69**, 2510 (1996).
[19]S. Reggiani, M. Valdinoci, L. Colalongo, M. Rudan, G. Baccarani, A. D. Stricker, F. Illien, N. Felber, W. Fichtner, and L. Zullino, IEEE Trans. Electron Devices **49**, 490 (2002).
[20]D. B. M. Klaassen, Solid-State Electron. **35**, 953 (1992).
[21]D. B. M. Klaassen, Solid-State Electron. **35**, 961 (1992).
[22]M. A. Green, J. Appl. Phys. **67**, 2944 (1990).
[23]N. W. Ashcroft and N. D. Mermin, Saunders College, Philadelphia (1976).